Flow Turbulence Combust (2016) 97:729–742
DOI 10.1007/s10494-016-9712-y

Effects of Synthetic jets on a D-Shaped Cylinder wake at a Subcritical Reynolds Number

N. Gao[1] · Y. Q. Li[1] · H. L. Bai[2,3,4] · C. J. Wu[1]

Received: 28 April 2015 / Accepted: 20 January 2016 / Published online: 15 February 2016
© Springer Science+Business Media Dordrecht 2016

Abstract Effects of synthetic jets on the wake of a D-shaped cylinder is investigated experimentally at a Reynolds number $Re_H = 47{,}000$, based on incoming free-stream velocity and the cylinder height (H). The synthetic jets are introduced immediately from the upper and lower trailing edges of the cylinder. The upper and lower synthetic jets are operated in an in-phase or anti-phase mode, and at a momentum ratio $C_\mu = 1.0\%$ and perturbation frequency $St_A = 0.11-0.37$. The cylinder wake with perturbation is examined in detail and compared with that without, based on smoke-wire flow visualization, pressure transducer and hotwire rake measurements, and data analyses of spectra, tempo-spatial cross-correlation and proper orthogonal decomposition (POD). Large-scale vortical structures in the cylinder wake are significantly modified by the synthetic jets perturbations, exhibiting symmetric or asymmetric patterns, depending on the perturbation frequency and phase relationship of the synthetic jets. These observations are internally correlated with the drag force variations.

Keywords Synthetic jet · D-Shaped cylinder wake · Flow control

1 Introduction

Flow around bluff bodies is prevalently encountered in engineering applications such as offshore struts, cable-stayed bridges and heavy trucks. A D-shaped cylinder has been considered as one of the basic models of the bluff-bodies (e.g. [1, 2]). Flow around a D-shaped

✉ H. L. Bai
honglei.bai@ust.hk

1 School of Aeronautics and Astronautics, Dalian University of Technology, Dalian 116024, China

2 State Key Laboratory of Aerodynamics, Mianyang 621000, China

3 Department of Mechanical Engineering, University of Melbourne, Parkville, VIC 3010, Australia

4 Present address: Department of Civil and Environmental Engineering, The Hong Kong University of Science and Technology, Clear Water Bay, Kowloon, Hong Kong

cylinder involves boundary layer, shear layer and vortex dynamics (e.g. [3]), and is featured by fixed flow separation points at the trailing edges due to the abrupt geometric change.

Manipulating shear layers separated from the trailing edges of a D-shaped cylinder, either passively or actively, can lead to pronounced modifications in vortical structures and, consequently, in fluid forces acting on the bluff body [1, 4–12]. A passive device, consisting of small tabs along the spanwise direction, was deployed by Park et al. [1] on the upper and lower trailing edges of a D-shaped cylinder, to perturb the vortex shedding. With optimum size and spacing, these small tabs dislocated the process of vortex shedding, thus resulting in significantly reduced vortical strength and substantially increased vortex formation length as well as wake width. A small circular cylinder placed downstream of the trailing edge of a D-shaped cylinder can drastically disturb the development of shear layers, elongate the bubble circulation and increase the base pressure (or reduce the drag force) [8, 9]. An effective approach to actively intervene in the shear layers is to introduce periodic perturbations at the trailing edges of a D-shaped cylinder. In a numerical simulation, Palei and Seifert [6] investigated effects of periodic excitation from synthetic jets on the wake of a D-shaped cylinder at a low Reynolds number $Re_H = 150$, based on incoming free-stream velocity and the cylinder height (H). Their synthetic jets had a large momentum ratio $C_\mu > 2\%$. The so-called 'lock-in' phenomenon, together with an increased drag force, was observed when the forcing frequency was approaching the natural shedding frequency of vortices. Palei and Seifert [6] also observed pronounced changes in flow patterns with perturbation, based on proper orthogonal decomposition (POD) analyses. Also using synthetic jets ($C_\mu > 0.5\%$) issued immediately from the upper and lower trailing edges, Pastoor et al. [7] managed, in an open-loop control scheme, to postpone the formation of vortex streets and achieved a reduction in time-averaged drag force by 15% ($Re_H = 23{,}000-70{,}000$). The synthetic jets used by Pastoor et al. [7] were operated in an in-phase mode and at a perturbation frequency $St_A = 0.15$, about $2/3St_o$, where St_o is the normalized vortex shedding frequency in the natural wake. They noted that the anti-phase perturbation was unsuitable for effective drag reduction, though without further discussions. Based on a similar setup to Pastoor et al. [7], Krajnovic and Fernandes [10] and Han and Krajnovic [11] performed extensive numerical investigations ($Re_H = 2{,}000-23{,}000$, $C_\mu = 3\%$ and $St_A = 0.045-0.17$) and observed good agreements between the numerical and experimental data. Recently, Parkin et al. [12] conducted large eddy simulations on a D-shaped cylinder wake ($Re_H = 23{,}000$, $C_\mu = 0.8\%$ and $St_A = 0.09-0.135$), focusing on transient wake analyses via dynamic mode decomposition (DMD) method. They achieved the maximum drag reduction (20%) at $St_A = 0.11$ under the in-phase perturbation and observed symmetric vortices in the near wake, which effectively extended the mean circulation bubble and thereby recovered the base pressure and reduced the drag force.

This study aims to investigate experimentally effects of synthetic jets on the vortical structures in a D-shaped cylinder wake. Both in-phase and anti-phase perturbations are conducted at a momentum ratio $C_\mu = 1.0\%$ and perturbation frequency $St_A = 0.11-0.37$. The D-shaped cylinder wake with perturbation will be examined and compared to that without, based on comprehensive measurements of smoke-wire flow visualization, pressure transducer and hotwire rake, and data analyses of power spectra, tempo-spatial cross-correlation and POD. Section 2 describes experimental details. Results and discussions are given in Section 3. This study is concluded in Section 4.

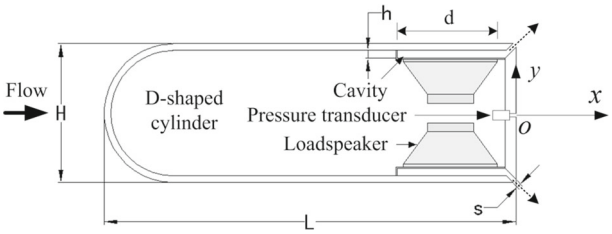

Fig. 1 Schematic of the D-shaped cylinder ($H = 63$ mm, $L = 188.5$ mm, $d = 45$ mm, $h = 3.5$ mm and $s = 2$ mm). The dotted arrows at the slot exits of the trailing edges indicate synthetic jets. Flow is left to right

2 Experimental Details

Experiments were conducted in an open-loop suction-type wind tunnel with a 0.7-m-long test section of 0.3 m ×0.3 m (width ×height). The maximum velocity of this tunnel is 30 m/s, with a turbulent intensity <0.5%. A D-shaped cylinder model made of acrylic (Fig. 1), having a length of $L = 188.5$ mm and a height of $H = 63$ mm, was placed horizontally in the test section, spanning the entire tunnel width (W) and thus resulting in a blockage of 21%. The cylinder model is supported by two aluminum bars at both ends. The distance between the leading edge of the cylinder model and the contraction exit of the tunnel is 0.11 m. Incoming free-stream velocity, corrected due to the large blockage [13], is $U_o = 11.7$ m/s, yielding a Reynolds number $Re_H = U_o H/\nu = 47{,}000$, where ν is kinematic viscosity of air. The Strouhal number defined by $St_o = f_o U_o/H$, where f_o is the dominant vortex-shedding frequency in the cylinder wake, is $St_o = 0.24$, very close to that (0.23) reported by Pastoor et al. [7]. Minimal effects of Reynolds numbers in the range of 23,000−70,000 have been shown by Pastoor et al. [7] and thus only $Re_H = 47{,}000$ was considered in the present investigation. The boundary layer thickness (based on $0.99U_o$ height) is about $0.15H$ above the side surface of the D-shaped cylinder, based on the time-averaged streamwise velocity profile measured using a single hotwire probe near the trailing edge at $x/H =$ -0.01. The coordinate system is located at the base center of the cylinder model (Fig. 1), with x, y and z corresponding to the streamwise, cross-flow and spanwise directions, respectively.

As shown in Fig. 1, two actuator-arrays, each having three spanwise-aligned loudspeakers, were mounted inside the cylinder model to generate synthetic jets through the two slots at the upper and lower trailing edges. The slot has a width $s = 2$ mm (or $s/H = 0.032$) and an inclination angle of 45° with respect to the streamwise direction, and spans a distance of 165 mm (i.e., $0.56W$) along the spanwise direction. Each loudspeaker has a cone of 45 mm in diameter. A 3.5 mm-high cavity connects the loudspeakers and the slot. The maximum output power of each loudspeaker is 4.4 Watts. The upper and lower sets of loudspeakers were driven by two individual sinusoidal voltages, which were generated by a voltage generator (ATTEN ATF20E) and amplified via two separate amplifiers (TDA7492). Thus, phase shift (φ) between these two sets of synthetic jets is easily adjustable. At $\varphi = 0$, the upper and lower sets of synthetic jets blow or suck simultaneously or, in other words, they work in an in-phase mode; at $\varphi = \pi$, the upper set blows and the lower set sucks or otherwise, that

is, they work in an anti-phase mode. Perturbation strength of the synthetic jets is characterized by the momentum ratio (C_μ) between the synthetic jets and the incoming flow (e.g., [7]), viz.,

$$C_\mu = 2(\frac{1}{2}\rho u_{A,rms}^2 s)/(\frac{1}{2}\rho U_o^2 H) = 2(s/H)(u_{A,rms}^2/U_o^2), \quad (1)$$

where ρ is air density and $u_{A,rms}$ is the root-mean-square (*rms*) value of the jet exit velocity (u_A) during the blowing period, measured using a single-wire hotwire probe (see details later) placed immediately at the center of the slot exit in stationary air. The hotwire was calibrated in-situ in the wind tunnel. The factor 2 in (1) accounts for both sets of synthetic jets at the upper and lower trailing edges. The driving voltages of the two sets of loudspeakers were adjusted carefully and documented before the tests, ensuring that the synthetic jets produced the same $u_{A,rms}$ within ±3% uncertainty at different operation frequencies (f_A).

The technique of smoke-wire flow visualization was employed to visualize instantaneous flow structures in the cylinder wake with and without perturbation. A stainless steel wire (diameter $d_o = 0.1$ mm), strained and attached to aluminum electrodes outside of the tunnel, was vertically placed at $x/H = 0.2$ downstream of the cylinder model. The steel wire was coated by a mixed liquid (70% paraffin + 30% kerosene) and then heated by a direct current with a maximum of 3 Amperes from a tailor-made circuit. Consequently, the heated mixture produced smoke filaments tracing the flow structures. A Canon 5D MKII camera was used to capture the visualized flow structures, with illumination from a flash. A digital timing circuit was used to synchronize the heating, illumination and capturing. It is worth noting that the present experiment of smoke-wire flow visualization was carried out at a Reynolds number $Re_{do} = U_o d_o/\nu \approx 75$, which is much larger than in the literature, and we obtained clearly vivid flow structures with and without perturbation (see Section 3); more details on this technique can be found in [14].

Streamwise fluctuating velocities, u, at $x/H = 5$ in the cylinder wake were measured using a hotwire rake, which comprises 15 equally-separated single-wire probes and covers a range of y/H = -1.5−1.5 along the cross-flow direction. The sensing element of each hotwire probe is a tungsten wire of 4.5 μm diameter and approximately 1.2 mm length. The hotwires were operated through a constant temperature anemometer (CTA, HANGHUA), with an overheat ratio of 1.8 used. The signals from the hotwires were offset, low-pass-filtered at a cutoff frequency of 2 kHz, and then sampled at a frequency of 2048 Hz using a 16-bit analogue-to-digital converter (NI, PCI-6014). The sampling time for each record is 150 s, ensuring the uncertainty of ±1.0% for the *rms* value of u. No calibration was carried out for the hotwires since only correlations between the raw signals were calculated.

Moreover, strain gauges (BF350-3AA) attached to the surface of the two supporting aluminum bars were employed to measure drag force acting on the cylinder model with and without perturbation. Signals from the strain gauges were amplified with a gain of 100 before being sampled under similar settings to the hotwire measurement. Time-averaged drag force coefficient is defined by $C_D = 2\overline{F}/(\rho U_o^2 HW)$, where $\overline{F}$ is the time-averaged drag force. The uncertainty of C_D is estimated to be ±2.5%. In addition, base pressure of the cylinder model was measured using a pressure transducer (CYH-130) mounted on the base center of the model (Fig. 1). The pressure tap has a diameter of 0.8 mm and a length of 3.0 mm. The transducer was calibrated using a water manometer (YJB-2500) with a resolution of 0.1 Pa. The static pressure coefficient has an uncertainty of ±2.0%. Fluctuating base pressures were measured in separate tests through connecting the pressure tap to a Panasonic microphone (WM-60B). The microphone has a flat response of 20−5,000 Hz and was calibrated using a microphone calibrator (HONGSHENG, HS6020) at 1000 Hz.

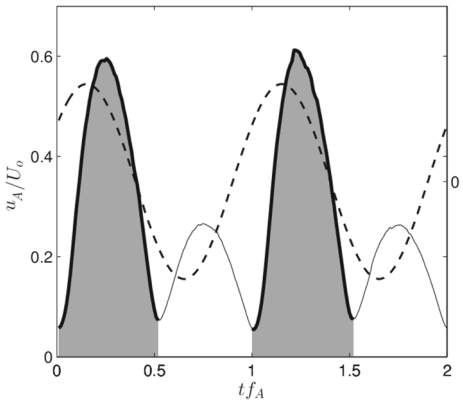

Fig. 2 Typical time-history of the exit velocity (u_A) for the synthetic jet. The blowing period of the jet is shaded. The dash line indicates the sinusoidal driving signal, which has an amplitude of 0.11 Volt and a frequency $f_A =$ 30 Hz

More details of the force and pressure measurements can be found in [15]. The signals from the microphone and the hot-wire rake were acquired simultaneously. As such, tempo-spatial cross-correlation between the fluctuating base pressure and streamwise velocities can be calculated.

3 Results and Discussions

3.1 Synthetic jet characteristics

Figure 2 presents a typical time-history of the normalized jet exit velocity u_A by U_o, together with the driving sinusoidal voltage signal. Only two periods of the signals are shown for the sake of clarity. The driving sinusoidal voltage has an amplitude of 0.11 Volt and a frequency of $f_A = 30$ Hz. In general, the jet exit velocity exhibits a periodic feature as expected. It can be seen that, at $0 < t^* = tf_A < 0.5$, the u_A/U_o increases rapidly and then decreases, again rapidly, with a peak of $u_A/U_o = 0.6$ at $t^* = 0.26$. Evidently, the blowing period (shaded in Fig. 2) was generated in the first-half period of the driving sinusoidal voltage, due to the pushing-forward motion of the loudspeaker cone. At $0.5 < t^* < 1$, i.e. in the second-half period of the driving sinusoidal voltage, the jet exit velocity climbs up first and then declines, with a peak ($u_A/U_o = 0.28$) at $t^* = 0.76$. This is the suction period produced by the withdrawing-backward motion of the loudspeaker cone. Here, the jet exit velocity during the suction is shown as positive rather than negative value in Fig. 2, which is ascribed to the inability of the single-wire hotwire in differentiating the flow direction. Further, the jet exit velocity in the suction period is much lower than that in the blowing, suggesting that a net momentum be generated by the synthetic jets [16]. Note that there is a delay ($\Delta t^* \approx 0.11$) between the driving sinusoidal voltage and jet exit velocity, due to the latency of the loudspeaker cone.

3.2 Drag force variations

Figure 3 shows variations of C_D/C_{Do} with St_A at $C_\mu = 1.0\%$, where C_{Do} denotes time-averaged drag coefficient without perturbation and St_A is defined by $St_A = f_A H/U_o$. For the in-phase perturbation, C_D was reduced by about 5% at the relatively low St_A (<0.2),

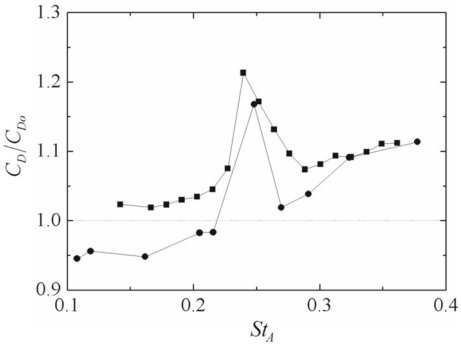

Fig. 3 Variations of C_D/C_{Do} with St_A at $C_\mu = 1.0\%$: •, in-phase perturbation; □, anti-phase. $Re_H = 47{,}000$

compared with that without perturbation. Pastoor et al. [7] observed minor drag reduction at $St_A = 0.15$ and C_μ <0.2%. For the anti-phase perturbation, however, C_D was increased at the relatively low St_A. At the relatively large St_A (>0.2), C_D was largely increased with increasing St_A, irrespective of the phase relationship between the upper and lower sets of synthetic jets. Particularly, C_D/C_{Do} exhibits a dominant peak at $St_A = 0.25$, which is very close to St_o, that is, the time-averaged drag of the D-shaped cylinder was increased mostly when the perturbation frequency was approaching the natural frequency of vortex shedding. The maximum increase in C_D is about 22% for the anti-phase perturbation, about 5% larger than that of the in-phase perturbation. These observations are ascribed to the occurrence of the 'lock-in' phenomena [6, 17, 18], where the vortical structures in the cylinder wake were sensitively and vigorously excited. At the relatively large perturbation frequency St_A (>0.3), drag increase is observed and C_D/C_{Do} grows gradually with increasing St_A.

3.3 Perturbed vortical structures

Without perturbation, the D-shaped cylinder wake exhibits typical von Karman vortex streets, consisting of staggered counter-rotating vortices alternately evolving downstream. This has been clearly demonstrated in Fig. 4a using the smoke-wire flow visualization technique. Shear layers embracing the primary vortices, together with small secondary vortices, have been visualized by the smoke filaments. The free stream flow, as indicated by the smooth smoke filaments, was entrained into the wake by these vortices. Once the perturbation from the synthetic jets was applied, there are pronounced changes in the cylinder wake, particularly in the patterns of the dominant vortices. In Fig. 4b and c, where the in-phase perturbation was introduced at $St_A = 0.16$ and 0.24, respectively, a pair of symmetric vortices was identified immediately downstream of the cylinder. As a result of that, the naturally alternating shear-layer development, rollup and shedding processes have been retarded. In other words, the in-phase perturbation delayed the transition from the shear layer mode to the asymmetric wake mode [7]. In the present study, an increased time-averaged base pressure (cf. [15]) was observed when the in-phase perturbation was applied at $St_A = 0.16$, indicating a reduction in the drag force (Fig. 3), in line with observations by Pastoor et al. [7] and Parkin et al. [12]. Further downstream (Fig. 4b & c), the pair of symmetric vortices became asymmetric, developing alternately downstream. On the other hand, once the anti-phase perturbation was applied, the staggered vortex street in the cylinder wake was greatly enhanced, as shown in Fig. 4d ($St_A = 0.16$) and (e) (0.24). The shear layer appears rolling

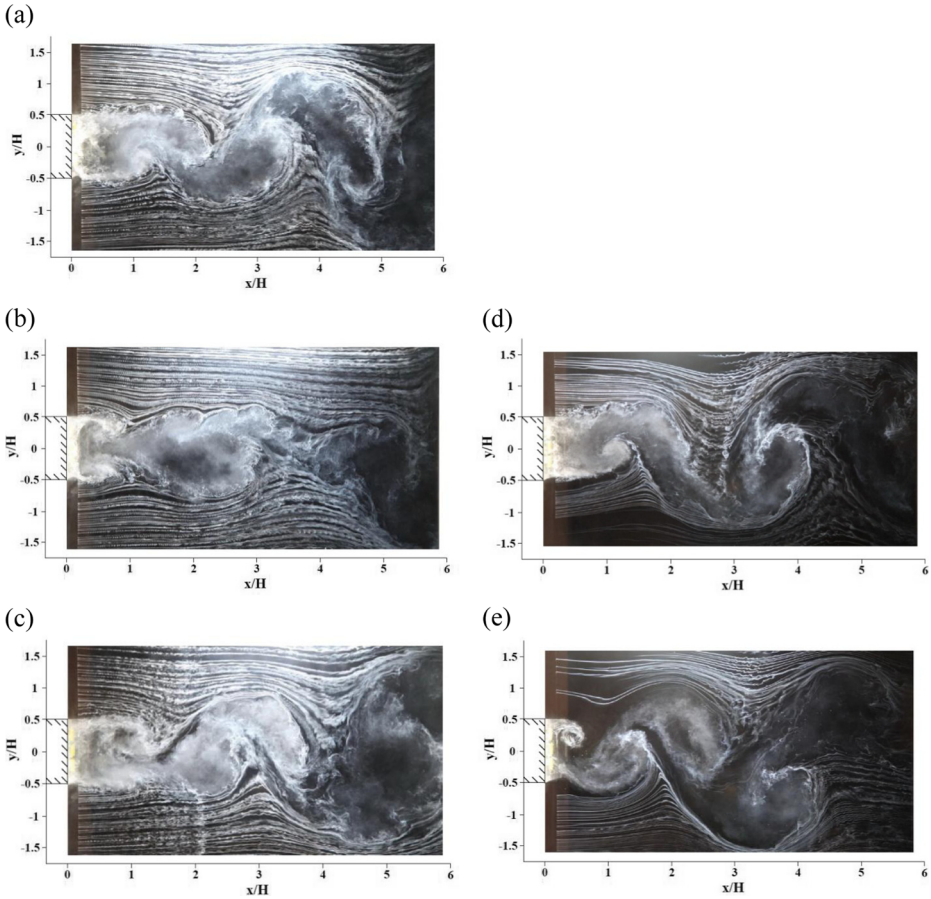

Fig. 4 Vortex streets in the wake of a D-shaped cylinder: **a** without perturbation; **b** with in-phase perturbation at $C_\mu = 1.0\%$ and $St_A = 0.16$; **c** in-phase, 1.0% and 0.24; **d** anti-phase, 1.0% and 0.16; and **e** anti-phase, 1.0% and 0.24. Flow is left to right. $Re_H = 47{,}000$

up immediately downstream of the trailing edges, particularly in the case of $St_A = 0.24$ (Fig. 4e) where the 'lock-in' phenomena occurred, indicating the strong synchronization between the anti-phase perturbation and the vortex shedding. This is internally connected to the drag force variations (Fig. 3).

Based on the fluctuating streamwise velocities (u) measured simultaneously via the two hotwires located at $y/H = \pm 1$ in the hotwire rake, their power spectra (E_u), co-spectra and phases were calculated and presented in Fig. 5. The dominant vortex shedding frequency (f) in the cylinder wake can be easily detected in the E_u distributions. Without perturbation, there is a pronounced peak at $St_o = 0.24$ in the E_u (Fig. 5a). Due to the alternating nature of the vortex shedding, a noticeable peak at $St_o = 0.24$ can also be identified with easy in the co-spectra of u (Fig. 5b), with a phase of π (Fig. 5c) between the upper ($y/H = 1$) and lower $u(y/H = -1)$. Note that a resonant frequency at $2St_o$ is discernible

in the E_u and the co-spectra. With the in-phase perturbation at $C_\mu = 1.0\%$ and $St_A = 0.16$, a dominant peak was detected at St_A in the E_u (Fig. 5d) and the co-spectra (Fig. 5e); on the other hand, the peak at St_o was largely retreated, indicating the suppressed vortex shedding. Further, we can see a phase lag of around 2 Radians at St_A (Fig. 5f), suggesting the modulated alternation of vortex shedding in the perturbed wake. These observations are consistent with that in the smoke-wire flow visualization (Fig. 4b). Based on the DMD analysis, Parkin et al. [12] found that periodic perturbations introduced an additional mode into the near wake, rather than displacing the natural mode of vortex shedding. The low perturbation frequency St_A allows the additional mode to develop coherently and meanwhile coexist with the natural mode. Once the anti-phase perturbation at $C_\mu = 1.0\%$ and $St_A = 0.24$ was apllied, a dominant peak at St_A took place in the E_u (Fig. 5g) and the co-spectra (Fig. 5h), with a phase lag of π Radians observed (Fig. 5). This is resultant from the synchronization or 'lock-in' between the natural vortex shedding and the enforced anti-phase perturbation (Fig. 4e). The perturbed vortical structures in the cylinder wake can also be revealed from the tempo-spatial cross-correlation between the fluctuating base pressure $p(0, 0, t)$ and streamwise velocities $u(5H, y, t)$ by the 15 hotwires in the rake located at $x/H = 5$. Figure 6 presents the contour maps of the cross-correlation function

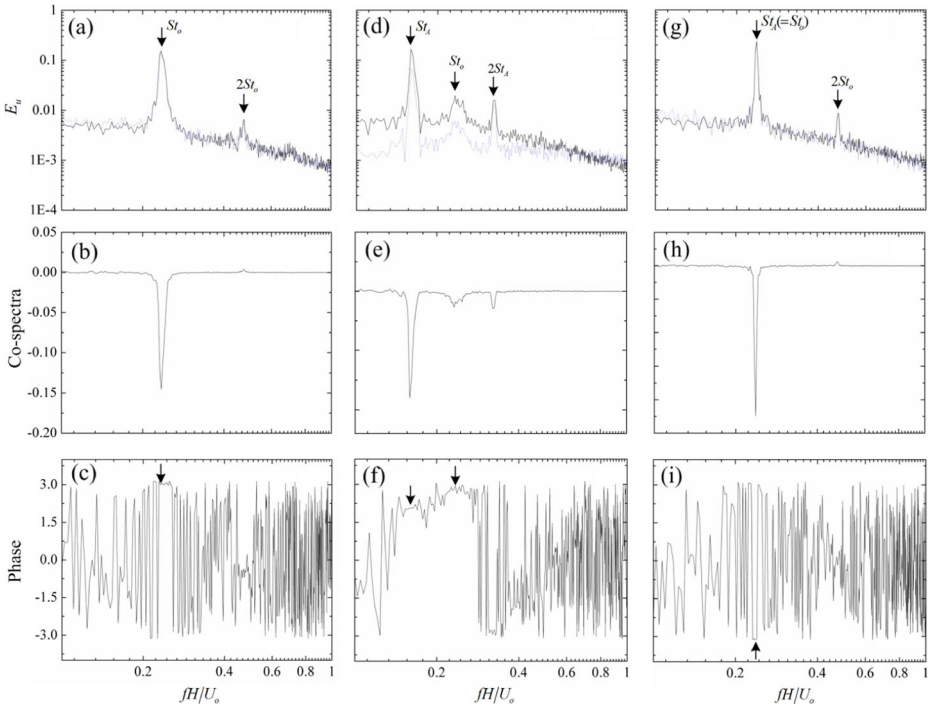

Fig. 5 Power spectra E_u (first row: a, d and g; —:$y/H = 1$, –:$y/H = -1$), Co-spectra (second row: b, e and h) and Phase (third row: c, f and i) of the fluctuating streamwise velocities (u) at $x/H = 5$ for the turbulent wake without perturbation (first column: a, b and c), with in-phase perturbation at $C_\mu = 1.0\%$ and $St_A = 0.16$ (second column: d, e and f), and with anti-phase perturbation at $C_\mu = 1.0\%$ and $St_A = 0.24$ (third column: g, h and i). $Re_H = 47{,}000$

$\rho_{pu}(\tau) = \overline{p(0,0,t)u(5H,y,t+\tau)}/p_{rms}u_{rms}$ with and without perturbation, where τ is the time delay between the fluctuating wall pressure and streamwise velocities, and p_{rms} and u_{rms} are the corresponding *rms* values of p and u, respectively. It can be seen that, without perturbation, the $\rho_{pu}(\tau)$ contours exhibit staggered arrangement (Fig. 6a); they are

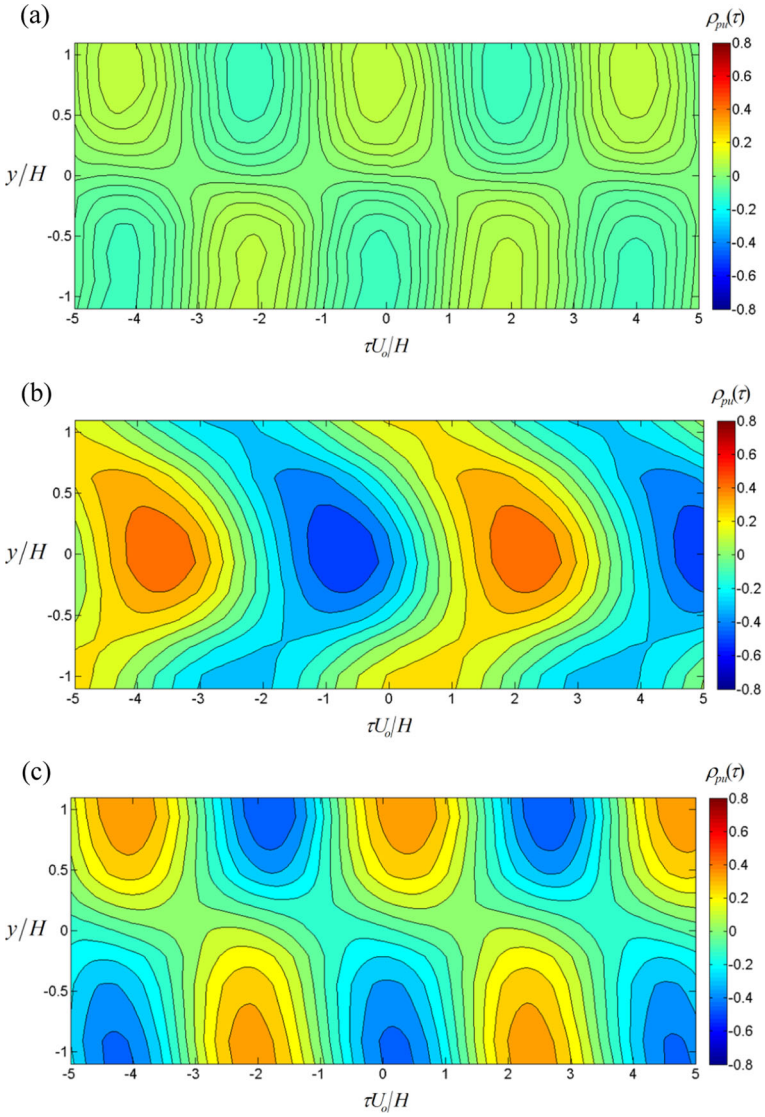

Fig. 6 Contour maps of the cross-correlation function $\rho_{pu}(\tau) = \overline{p(0,0,t)u(5H,y,t+\tau)}/p_{rms}u_{rms}$ between the base pressure p and streamwise velocities u from the 14 hotwires at $x/H = 5$: (a) case 1:without perturbation; (b) case 2: with in-phase perturbation at $C_\mu = 1.0\%$ and $St_A = 0.16$; and (c) case 3:anti-phase, 1.0% and St_A =0.24. $Re_H = 47{,}000$

Table 1 Energy fraction in the lower POD modes: case 1, without perturbation; case 2, in-phase perturbation at $C_\mu = 1.0\%$ and $St_A = 0.16$; and case 3, anti-phase perturbation at $C_\mu = 1.0\%$ and $St_A = 0.24$

	Mode 1	Mode 2	Mode 3	Modes 1-3
Case 1	33%	20%	9%	62%
Case 2	35%	19%	10%	64%
Case 3	29%	21%	10%	60%

anti-symmetric about $y/H = 0$, consistent with the noticeable feature of the cylinder wake (Fig. 4a). However, once the perturbation was applied, either in the in-phase or anti-phase mode, the $\rho_{pu}(\tau)$ contours (Fig. 6b & c) display distinct patterns from that without perturbation. For the in-phase perturbation at $St_A = 0.16$, the $\rho_{pu}(\tau)$ contours show alternating pattern along the time axis, and they are symmetric about $y/H = 0$, indicating a symmetric near-wake and further echoing the observation from the smoke-wire flow visualization (Fig. 4b). For the anti-phase actuation at $St_A = 0.24$, the $\rho_{pu}(\tau)$ contours have a similar pattern to that in Fig. 6a; however, the value of correlation coefficient $\rho_{pu}(\tau)$ is greatly increased, indicating that the vortex street was vigorously excited. Further, it can be seen that the horizontal spacing between the maxima of $\rho_{pu}(\tau)$ in Fig. 6b is larger than that in Fig. 6c, suggesting that the convection velocity of the vortices in the symmetric pattern is smaller than that in the asymmetric pattern. This may indicate that the formation of vortex street was postponed by the in-phase perturbation (Fig. 5f; [7]).

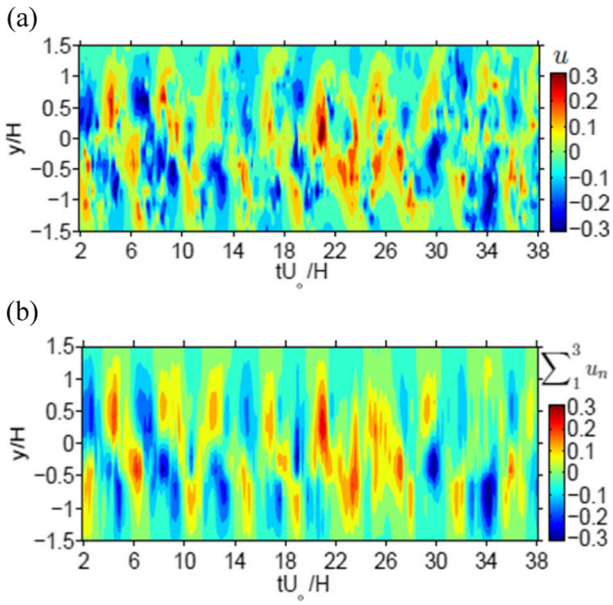

Fig. 7 Streamwise fluctuating velocity u in the D-shaped cylinder wake without perturbation, measured using a hotwire rake at $x/H = 5$: (a) hotwire-measured u; and (b) reconstructed u based on first 3 POD modes, i.e., $\sum_1^3 u_n$

3.4 Proper orthogonal decomposition

The POD method is widely used to extract energetic large-scale coherent structures from turbulent flows. Here, fluctuating streamwise velocities $u(x = 5H, y, t)$, measured using the hotwire rake, are decomposed into different modes $u_n(y, t)$, based on the POD method [19], viz.,

$$u(y,t) = \sum_{n=1}^{N} u_n(y,t) = \sum_{n=1}^{N} a_n(t)\Psi^{(n)}(y), \tag{2}$$

where N is the total number of POD modes and presently $N = 15$, and $a_n(t)$ is the temporal coefficient of the nth POD mode $\Psi^{(n)}(y)$. Further, $\Psi^{(n)}(y)$ can be attained by solving an eigenvalue function $\int R(y, y', \tau = 0)\Psi^{(n)}(y') = \lambda_n \Psi^{(n)}(y)$, where $R(y, y', \tau)$ is a spatial correlation tensor defined by $R(y, y', \tau) = \overline{u(y,t)u(y', t+\tau)}$, and λ_n is the eigenvalue corresponding to $\Psi^{(n)}(y)$ and indicates the energy fraction of $\Psi^{(n)}(y)$ in terms of turbulent kinetic energy.

Table 1 presents energy fraction in the lower POD modes for the cylinder wake with and without perturbation. For the natural wake (case 1), the POD mode 1, 2 and 3 has the energy fraction of 33%, 20% and 9%, respectively. These three modes have contributed up to 62% of the total energy, suggesting that these lower modes play an important role in the dynamics of the wake structures. In fact, as illustrated in Fig. 7, the reconstructed streamwise fluctuating velocity u based on modes 1-3, i.e., $\sum_1^3 u_n$ (Fig. 7b), exhibits similar staggered patterns to that from the raw u (Fig. 7a). Once the in-phase perturbation is applied at $C_\mu = 1.0\%$ and $St_A = 0.16$ (case 2), the energy fraction of modes 1 and 3 are increased marginally by 2% and 1%, respectively, and that of mode 2 is reduced by 1%. The energy fraction of modes 1-3 is 64% for the perturbed wake (case 2), 2% higher than that of their unperturbed counterpart. On the other hand, with the anti-phase perturbation at $C_\mu = 1.0\%$ and $St_A = 0.24$ (case 3), the energy fraction of mode 1 is reduced by 4%, and that of mode 2 is increased by 1%, with that of mode 3 remained unchanged; the energy fraction of modes 1-3 is 60%, 2% lower than of their unperturbed counterpart. These observations in case 3 are actually opposite to that in case 2, suggesting distinct modifications of the flow structures.

It is of interest to examine characteristics of the mode shape $\Psi^{(n)}$ with and without perturbation. Figure 8 presents the mode shape $\Psi^{(n)}$ for the lower three POD modes with different perturbation, in comparison to that without. For the natural wake of the cylinder (case 1), the 1st POD mode (Fig. 8a) is anti-symmetric about the centerline at $y/H = 0$, which is internally associated with the dominant alternating features in the wake. However, the 2nd POD mode (Fig. 8b) appears symmetric about the centerline ($y/H = 0$), with the peak at the center, suggesting the occurrence of symmetric vortex pair in the natural wake. The 3rd POD mode is asymmetric about the centerline, which is perhaps linked to the secondary vortices in the wake. Once the perturbation is introduced, there are significant changes in the 1st and 2nd POD modes, as shown in Fig. 8a & (b), respectively. With the in-phase perturbation at $C_\mu = 1.0\%$ and $St_A = 0.16$ (case 2), the 1st mode displays a roughly symmetric distribution about the centerline, whereas the 2nd mode an anti-symmetric distribution about the centerline. This indicates that symmetric flow structures are dominant in the cylinder wake under the in-phase perturbation at $C_\mu = 1.0\%$ and $St_A = 0.16$. With the anti-phase perturbation at $C_\mu = 1.0\%$ and $St_A = 0.24$ (case 3), both 1st and 2nd modes exhibit asymmetric distributions (Fig. 8a & b). These observations from the lower POD modes are consistent with that

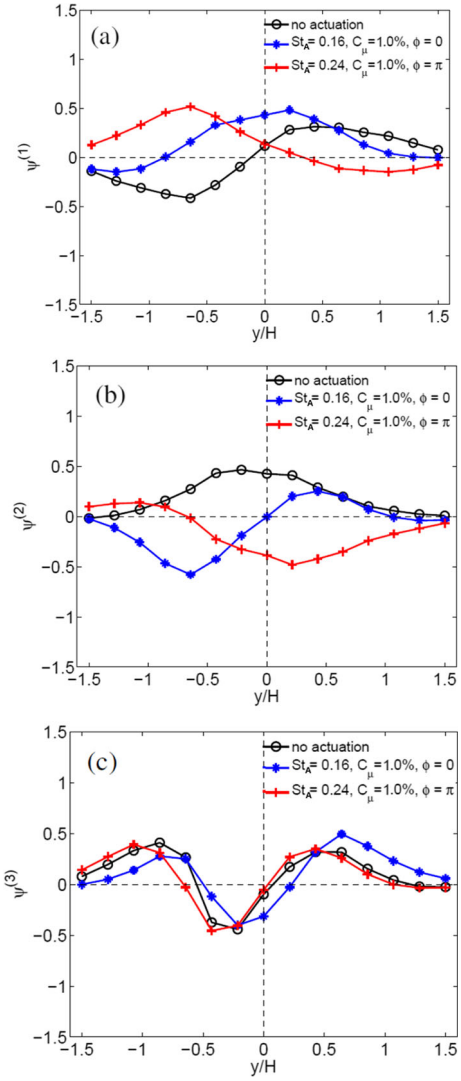

Fig. 8 Mode shape ($\psi^{(i)}$) for the lower ith POD mode: (a), $\psi^{(1)}$; (b), $\psi^{(2)}$; and (c) , $\psi^{(3)}$

from the smoke-wire flow visualization (Fig. 4) and cross-correlation (Fig. 6). There is no significant change for the 3rd mode (Fig. 8c) with perturbation from that without.

The reconstructed u based on mode 1, 2 or 3, i.e., u_n ($n = 1$, 2 or 3) in Fig. 9 is tightly connected to the observations in the corresponding mode shape (Fig. 8). For the natural wake (case 1), u_1 displays an anti-symmetric pattern (Fig. 9a), associated with the staggered fashion of the vortex street, about the centerline. u_2 is symmetric (Fig. 9b) whilst u_3 is asymmetric about the centerline (Fig. 9c). Once the in-phase perturbation at $C_\mu = 1.0\%$ and $St_A = 0.16$ is applied, u_1 exhibits symmetric (Fig. 9d) and u_2 is anti-symmetric (Fig. 9e)

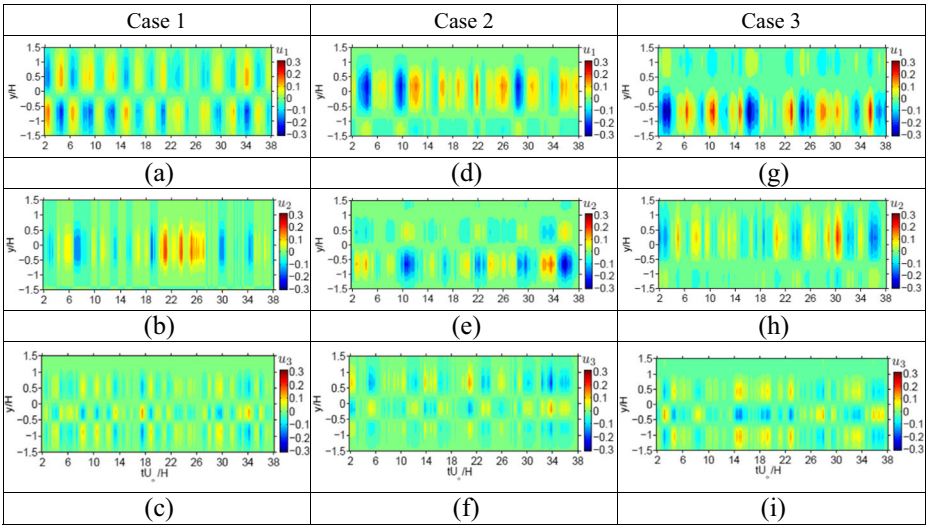

Fig. 9 Reconstructed u based on mode 1, 2 or 3, i.e., u_n (n = 1, 2 or 3): case 1, without perturbation; case 2, in-phase perturbation at $C_\mu = 1.0\%$ and $St_A = 0.16$; and case 3, anti-phase perturbation at $C_\mu = 1.0\%$ and $St_A = 0.24$

about the centerline. With the anti-phase perturbation at $C_\mu = 1.0\%$ and $St_A = 0.24$, u_1 and $u_2$appear asymmetric (Fig. 9g, h) about the centerline.

4 Conclusions

The D-shaped cylinder wake was perturbed using synthetic jets issued from the 2 mm-wide slots located immediately at the trailing edges. The experiments were conducted in a wind tunnel at $Re_H = 47{,}000$. The synthetic jets were operated at a perturbation strength (i.e., $C_\mu = 1.0\%$) and a wide range of perturbation frequency (i.e., $St_A = 0.11-0.37$), with an in-phase or anti-phase mode employed. Different measurement techniques and data analysis methods were performed in the study, including smoke-wire flow visualization, pressure transducer, hotwire rake, spectra, cross-correlation and POD. The large-scale vortical structures in the cylinder wake were significantly modified by the perturbations of the synthetic jets, exhibiting noticeably distinct behaviors from that without perturbation. With the in-phase perturbation at $St_A = 0.16$ (about 30% lower than St_o), the vortical structures displayed symmetric patterns in the downstream vicinity of the cylinder; the vortex pairs evolved slower than that without perturbation, and became asymmetric further downstream. This flow pattern contributed to the drag reduction obtained at the low St_A (<0.2). The cross-correlation function $\rho_{pu}(\tau)$ and the POD mode shape $\Psi^{(1)}$ exhibit symmetric distributions about the centerline. With the anti-phase perturbation at $St_A = 0.16$ and 0.24, particularly in the latter case where $St_A \approx St_o$, the 'lock-in' phenomena took place and the vortical structures were vigorously excited, displaying a remarkable alternating pattern in the near wake. The distributions of $\rho_{pu}(\tau)$ and $\Psi^{(1)}$ are symmetric about the centerline.

Acknowledgments This work is supported by State Key Laboratory of Aerodynamics through grant SKLA20130102, National Natural Science Foundation of China through grant 11302062, the '973 plan' of China through grant 2014CB744100, and Dalian University of Technology through grant DUT14LK07.

References

1. Park, H., Lee, D., Jeon, W., Hahn, S., Kim, J., Kim, J., Choi, J., Choi, H.: Drag reduction in flow over a two-dimensional bluff body with a blunt trailing edge using a new passive device. J. Fluid Mech. **563**, 389–414 (2006)
2. Choi, H., Jeon, W.-P., Kim, J.: Control of flow over a bluff body. Annu. Rev. Fluid Mech. **40**, 113–139 (2008)
3. Meliga, P., Pujals, G., Serre, E.: Sensitivity of 2-D turbulent flow past a D-shaped cylinder using global stability. Phys. Fluids **24**(061701) (2012)
4. Siegel, S., Cohen, K., Seidel, J., Mclaughlin, T.: Two dimensional simulation of a feedback controlled D-cylinder wake. 35th AIAA Fluid Dynamics Conf. Exhibit, 6-9 Toronto, Ontario Canada, paper no. AIAA, 2005–5019 (2005)
5. Stalnov, O., Palei, V., Fono, I., Cohen, K., Seifert, A.: Experimental estimation of a D-shaped cylinder wake using body-mounted sensors. Exp. Fluids **42**, 531–542 (2007)
6. Palei, V., Seifert, A.: Effects of periodic excitation on the flow around a D-shaped cylinder at low Reynolds numbers. Flow Turbulence Combust **78**, 409–428 (2007)
7. Pastoor, M., Henning, L., Noack, B.R., King, R., Tadmor, G.: Feedback shear layer control for bluff body drag reduction. J. Fluid Mech. **608**, 161–196 (2008)
8. Thiria, B., Cadot, O., Beaudoin, J.-F.: Passive drag control of a blunt trailing edge cylinder. J. Fluids Struct. **25**, 766–776 (2009)
9. Han, X., Krajnovic, S.: Very large eddy simulation of passive drag control for a D-shaped cylinder. J. Fluids Eng., Trans. ASME **135**(101102) (2013)
10. Krajnovic, S., Fernandes, J.: Numerical simulation of the flow around a simplified vehicle model with active flow control. Int. J. of Heat Fluid Flow **31**(1), 192–200 (2011)
11. Han, X., Krajnovic, S.: Study of active flow control for a simplified vehicle model using the PANS method. Int. J. Heat Fluid Flow **42**, 139–150 (2013)
12. Parkin, D.J., Thompson, M.C., Sheridan, J.: Numerical analysis of bluff body wakes under periodic open-loop control. J. Fluid Mech. **739**, 94–123 (2014)
13. West, G.S., Apelt, C.J.: The effect of tunnel blockage and aspect ratio on mean flow past a circular cylinder with Reynolds number between 10^4 to 10^5. J. Fluid Mech. **14**, 361–377 (1982)
14. Liu, X.H., Gao, N.: An improved smoke-wire visualization technique for flow with relatively high velocities. 4th Int. Conf. Exp. Fluid Mech. Beijing , China Aug. 12–15 **2014** (2014)
15. Li, Y.Q., Bai, H.L., Gao, N.: Drag of a D-shaped bluff body under small amplitude harmonic actuation. Theor. Appl. Mech. Lett. **5**, 35–38 (2015)
16. Glezer, A., Amitay, M.: Synthetic jets. Annu. Rev. Fluid Mech. **34**, 503–529 (2002)
17. Armstrong, B.J., Barnes, F.H.: The effect of a perturbation on the flow over a bluff cylinder. Phys. Fluids **29**(7), 2095–2102 (1986)
18. Griffin, O.M.: Flow similitude and vortex lock-on in bluff body near-wake. Phys. Fluids A **1**(4), 697–703 (1989)
19. Bonnet, J.P., Delville, J., Glauser, M.N., Antonia, R.A., Bisset, D.K., Cole, D.R., Fiedler, H.E., Garem, J.H., Hilberg, D., Jeong, J., Kevlahan, N.K.R., Ukeiley, L.S., Vincendeau, E.: Collaborative testing of eddy structure identification methods in free turbulent shear flows. Exp. Fluids **25**, 197–225 (1998)